Journal of Analytical and Applied Pyrolysis 109 (2014) 47–55

Contents lists available at ScienceDirect

Journal of Analytical and Applied Pyrolysis

journal homepage: www.elsevier.com/locate/jaap

Torrefaction of some Nigerian lignocellulosic resources and decomposition kinetics

Olumuyiwa A. Lasode[a,*], Ayokunle O. Balogun[b], Armando G. McDonald[b]

[a] Department of Mechanical Engineering, Faculty of Engineering and Technology, University of Ilorin, Ilorin, Nigeria
[b] Department of Forest, Rangeland and Fire Sciences, University of Idaho, Moscow, ID 83844-1132, USA

ARTICLE INFO

Article history:
Received 1 January 2014
Accepted 17 July 2014
Available online 1 August 2014

Keywords:
Torrefaction
Decomposition kinetics
Biomass
Renewable energy
Bio-oil

ABSTRACT

Torrefaction experiments were carried out on some Nigerian woody (*Albizia pedicellaris* (AP), *Tectona grandis* (TK), *Terminalia ivorensis* (TI)) and non-woody (*Sorghum bicolour* glume (SBG) and stalk (SBS)) biomass resources. The influence of process conditions and consequent change in the elemental configuration of the biomass samples were observed. Biomass type played a dominant role in the solid yield recording 71% for woody and 58% for non-woody samples at 270 °C, while temperature showed the greatest influence with solid yield dropping from an average of 80% (at 240 °C) to 50% (at 300 °C). Both volatile matter and fixed carbon contents experienced significant changes after torrefaction and a decline in O/C ratio from 0.6 to 0.3 was noted. Among the woody biomass, TI experienced the highest increase in higher heating value (HHV) of approximately 38% as compared to AP (32%) and TK (32%), and was subsequently selected for decomposition kinetic study. The decomposition kinetics showed that activation energy ($E(\alpha)$) for the hemicellulose degradation stage ranged between 137 and 197 kJ mol^{-1} for conversion (α) between 0.1 and 0.24 implying that biomass kinetics within this decomposition region is a multi-step reaction. The GC/MS analytical technique revealed that the presence of levoglucosan was highest (7.1%) in woody biomass, while phenolic compounds made up more than one-third of the group of compounds identified.

1. Introduction

The global growing energy consumption, dwindling fossil fuel reserves and increasing environmental concerns relating to the use of petroleum products have inevitably led to an apparent quest for alternative and renewable energy sources. The notable ones include geothermal, wind, solar, biomass and wave energy; however, biomass has assumed a pivotal role because it is the only one that is reported to be carbon neutral and possess infinite sustainability potentials [1]. The wide variety and abundant availability of biomass wastes generated in the processing of raw biomass resources on the one hand, and the concomitant disposal challenges on the other hand, are among the factors that have continued to motivate keen interest in the utilization of lignocellulosic biomass as renewable energy resource.

Torrefaction, a thermochemical conversion process, has gained global attention as a viable pretreatment technology for biomass feedstock in gasification and co-combustion processes [2,3]. The production of high quality char for domestic heating and cooking through the technology of torrefaction has become a subject of scientific research and development [4,5]. Torrefied biomass resource could also be of practical importance in the metallurgical industry [6]. Though similar to pyrolytic conversion process in that it is conducted in an inert atmosphere or in the presence of limited air, other process conditions such as residence time, operating temperature and heating rates differ significantly. Torrefaction experiments are conducted at low heating rates (<100 °C min^{-1}), between 220 and 300 °C and approximately 1 hr residence time resulting in the production of a homogenous carbon-rich char [1]. The characteristic properties of torrefied biomass are substantially influenced by biomass type, particle size and mostly temperature [3,7].

Raw biomass is hydrophilic, heterogeneous in structure, and possesses high moisture content leading to poor combustion characteristics. Furthermore, the high O content of raw biomass has been implicated in smoke emission during combustion [1]. It has been observed that prolonged exposure to smoke emissions from the use of raw woody biomass; as is the case in most rural areas in developing countries, raises some health concerns that manifest in eye-related and respiratory complications [8,9]. Unfortunately, the harvest of woody biomass resources for fuelwood is still common-

* Corresponding author. Tel.: +234 8066778409; fax: +234 8055647409.
E-mail address: oalasode@yahoo.com (O.A. Lasode).

http://dx.doi.org/10.1016/j.jaap.2014.07.014
0165-2370/

place in Nigeria in spite of the various land degradation scenarios it also poses. Apparently, biomass residues have been reported to be enormously available in Nigeria. An estimate of 7 million m^3 of forestry wastes is generated annually from logging and sizing operations, while an FAO 2010 data estimated a total of 11.37 million tons of waste from sorghum cultivation [10,11]. Therefore, upgrading of biomass residues through torrefaction has an immense prospect in Nigeria as it could help curb the infamous act of tree felling and also transform the widespread biomass wastes generated to valuable biofuel products.

In the process of torrefaction, moisture and low molar mass organic compounds that are responsible for energy loss due to their endothermic behavior are liberated [12,13]. The hemicellulose fraction is decomposed alongside yielding a hydrophobic and a relatively homogenous product [1,3]. In addition, a change in the elemental configuration is engendered; leading to a reduction in both the O and H components and a significant increase in the C content [14]. Thus, the thermal and structural properties of biomass are enhanced making them suitable for applications such as domestic cooking, residential heating and co-firing options.

One of the product yields after torrefaction is the condensed liquid (bio-oil) from which various chemicals and fuels can be extracted [15]. The chemical composition of the bio-oil is of prime importance because information concerning what refinement process or upgrading technique might be needed can be gathered. Apparently, the composition of bio-oil from pyrolytic conversion of biomass has been investigated extensively [16–18]. Since temperature affects the formation and concentration of the chemical species in the liquid portion produced during thermochemical conversion processes, it becomes imperative to investigate the makeup of the bio-oil from torrefaction experiments. Given that not much effort has been seen in this direction, one of the objectives of this study therefore is to subject the condensed liquid from torrefaction process to GC/MS instrumental analysis.

The thermal decomposition of biomass involves a very complex chemical reaction that often defies a one-step kinetic scheme. It has been noted that multi-step mechanisms provide more accurate descriptions of the reaction processes that follow successive and parallel routes [7,19]. These are frequently encountered in the thermal treatment of biomass. Isoconversional methods also referred to as model-free techniques, have been improved upon to handle multi-step reactions. These evaluate kinetic parameters as a function of degree of conversion (α). They are implemented on the basis of multiple thermogravimetric analysis (TGA) measurements and the elimination of an assumption of any reaction model. Flynn–Wall–Ozawa (FWO) and Starink are two foremost model-free techniques that are commonly used in the calculation of kinetic data [20,21] and these will be used in this study.

The primary objective of this study was to investigate how varied torrefaction process conditions influence the yield distributions on some Nigerian hardwoods and non-woody biomass resources. The consequent chemical changes on the different biomass resources will also be monitored, while thermal decomposition kinetic studies will be performed on the hardwood, *Terminalia ivorensis*.

2. Materials and method

2.1. Materials

2.1.1. Biomass source

Biomass resources categorized into agricultural (non-woody) and forestry (woody) were obtained from a farm site (8°37′ N, 4°46′ E) and a timber processing plant (8°27′ N, 4°35′ E) in the city of Ilorin, Nigeria respectively in December 2012. The non-woody sample was *Sorghum bicolour* (SB, guinea corn), while the woody samples were tropical hardwoods namely: *Albizia pedicellaris* (AP), *Tectona grandis* (TK) and *T. ivorensis* (TI).

2.1.2. Harvesting and handling

The maturity period of the SB plant is six months. After harvesting and threshing, SB panicles and stems were air dried for about one month. The SB glumes (SBG) were handpicked, while the leaves on the SB stems were stripped off and the SB stalk (SBS) cut into a length of 0.305 m. Woodchips from the stem of forestry samples, with age between 40 and 45 years, were also produced and air dried for about one month. These were separately packed in polyethylene bags and transported to the Renewable Materials Laboratory at the University of Idaho.

2.1.3. Sizing, sieving and storage

Biomass resources described in Section 2.1.2 were milled in Thomas Wiley Laboratory Mill Model 4 to pass a 1 mm screen and then sieved into particle sizes ranges <0.25 mm, 0.25–0.5 mm and 0.5–1.0 mm. Thereafter they were all stored in Ziploc bags and kept in a desiccator at room temperature.

2.2. Methods

2.2.1. Proximate and elemental analyses

The method according to the British Standard BS EN 15148:2009 [22] was used for the evaluation of the content of volatile matter (VM). The ash content determination was carried out in a muffle furnace at 580 °C in accordance with the method of ASTM D1102-84 [23], while the moisture content (MC) measurement was performed on a HB 43-S Mettler Toledo moisture analyser. The fixed carbon content (FCC) was calculated by difference. Elemental analysis was conducted using CE 440 elemental analyser to determine C, H and N contents and O was calculated by difference.

2.2.2. Heating value

Higher heating value (HHV) of biomass samples, in triplicate, was determined using a Parr oxygen bomb calorimeter model 1341 according to the ASTM D5865-04 [24]. Biomass sample (1.0 g) was pelletized (6 mm Ø) on a Carver Laboratory hydraulic press to a pressure of 13.8 MPa and dried prior to charging the bomb.

2.2.3. Thermogravimetric analysis (TGA)

Thermogravimetric analysis (Perkin Elmer TGA-7, Massachusetts, USA) with N_2 purge gas (30 mL min^{-1}) was used for the decomposition tests. Samples (2–5 mg, <0.25 mm) were heated under non-isothermal conditions; temperature was held for 1 min at 323 K and subsequently ramped from 323 to 1173 K at 5, 10 and 20 K min^{-1}. Experiments were done in duplicate and good reproducibility was obtained. duplicate and good reproducibility was obtained.

2.2.4. Gas chromatography–mass spectrometry (GC–MS) analysis

A drop of the condensed liquid (bio-oil) (2–3 mg) released during torrefaction was placed in a 2 mL GC vial and diluted with 1.0 mL of methanol. The mixture was analyzed using a GC–MS_{EI} (FOCUS-ISQ ThermoScientific, San Jose, CA, USA), temperature profile: 50 °C (10 min) at 5 °C min^{-1} to 290 °C; GC capillary column: (ZB-1, 30 m, 0.25 mm Ø, Phenomenex, Torrence, CA, USA). The eluted compounds were identified with authentic standards, NIST 2008 library matching and by their mass spectra [25,26].

2.2.5. Torrefaction

Fig. 1 shows the laboratory scale set-up of the equipment that was used for torrefaction experiments. It consists of a tubular reactor (10 mm Ø × 305 mm, Swagelok cap fittings at both ends),

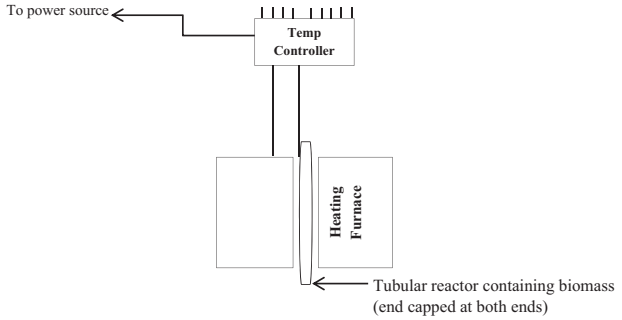

Fig. 1. Schematic diagram of laboratory scale set-up for torrefaction experiments.

digital temperature controller and a Supelco model 23800 tube furnace (90 W). Biomass (1.000 g) of known moisture content was loaded into an aluminum foil boat and placed into the reactor at varied residence time (15 and 30 min), operating temperature (240, 270, 300 °C) and particle size (<0.25, 0.25–0.5, and 0.5–1.0 mm). The operating parameters influenced the product yields which were determined gravimetrically using an offline method. This method entails measuring the initial mass (m_t) of the airtight sealed reactor containing the test sample prior to putting it in the heating furnace. After the torrefaction experiments were completed at the required residence time, the reactor was allowed to cool to room temperature, opened for volatiles to escape and the mass noted as (m_v). The difference between m_t and m_v gave the mass of the volatile yield (V_y). Thereafter the char yield (C_y) remaining in the aluminum boat was recovered and the mass noted. The difference between 100 and the volatile and char yields gave the liquid yield. This may be expressed as $100\% - V_y\% - C_y\% = L\%$.

where V_y, volatile yield, C_y, char yield and L, liquid yield.

3. Decomposition kinetic study

3.1. Model-free technique

Model-free techniques provide qualitative information on decomposition kinetics as activation energy (E) is evaluated at varying degrees of conversion (α). These methods presuppose that decomposition process progresses through a single-step reaction (reactant to product) at constant heating rate eliminating the need for an assumption of reaction mechanisms.

The global kinetic equation for solid-state decomposition rate may be written as,

$$\frac{d\alpha}{dt} = k(T)f(\alpha) \tag{1}$$

where the temperature dependent function is expressed as Arrhenius equation:

$$k(T) = A\exp^{(-E/RT)} \tag{2}$$

At constant heating rate $\beta = dT/dt$, combining Eqs. (1) and (2) and integrating gives the general single-step rate equation:

$$\int_0^{\alpha} \frac{d\alpha}{f(\alpha)} = g(\alpha) = \frac{A}{\beta}\int_{T_0}^{T} \exp^{(-E/RT)}dT = \left(\frac{AE}{\beta R}\right)p(x) \tag{3}$$

where A (min^{-1}) is the pre-frequency factor, R is the Boltzmann gas constant (8.314 J mol^{-1} K^{-1}), α is the degree of conversion, and $f(\alpha)$ is the reaction model which is a function of conversion. The term $p(x)$ is referred to as the temperature integral and it has no exact analytical solution. The approximations proposed by FWO [20] and Starink [21] were adopted for this study.

Table 1
Proximate and elemental analyses and higher heating value of biomass resources.

	Woody			Non-woody	
	AP	TK	TI	SBG	SBS
Proximate analysis[a] (wt%)					
VM	92.7	95.5	82.3	78.9	82.9
FCC[b]	5.61	3.8	17.4	13.6	13.8
Ash	1.68	0.7	0.32	7.54	3.25
Elemental analysis[a] (wt%)					
C	51.7	49.6	48.6	42.4	46.2
H	5.85	6.3	6.00	5.27	5.85
N	0.54	0.4	0.44	0.74	0.44
O[b]	42.0	43.7	45.0	51.6	47.6
HHV (MJ/kg)	20.1	19.8	17.3	16.4	17.9

[a] Dry-basis.
[b] Calculated by difference, HHV, higher heating value.

3.1.1. Flynn–Wall–Ozawa's (FWO) method

The FWO method is one of the notable model-free techniques commonly used for the determination of kinetic parameters [20]. The FWO method linearizes the temperature integral in Eq. (3) using Doyle's empirical approximation [27] as shown in Eq. (4).

$$\log p(x) \cong -2.315 + 0.457x \tag{4}$$

Taking logarithm of Eq. (3) and combining with Eq. (4) gives the FWO expression in Eq. (5).

$$\log\beta = \log\frac{AE}{g(\alpha)R} - 2.315 - 0.457\frac{E}{RT} \tag{5}$$

A plot of $\log\beta$ against the inverse of absolute temperature gives a slope from which the activation energy can be calculated (Eq. (6)) [28]

$$Slope \cong 0.457\frac{E}{R} \tag{6}$$

3.1.2. Starink's method

Starink [29] examined two iso-conversional techniques FWO and Kissinger–Akhira–Sunose (KAS)) and found out that both conform to the expression in Eq. (7).

$$\ln\left(\frac{\beta}{T^s}\right) = C_S - \frac{BE}{RT} \tag{7}$$

where for FWO $s = 0$, $B = 0.457$ and for KAS $s = 2$ and $B = 1$. Starink optimized the values for the constants s and B and proposed that $s = 1.8$, while $B = 1.0037$. It was reported that Starink's method was an order of magnitude more accurate than the other two iso-conversional methods [29]. Hence, Starink's method can be expressed as Eq. (8)

$$\ln\left(\frac{\beta}{T^{1.8}}\right) = C_S - 1.0037\frac{E}{RT} \tag{8}$$

A plot of $\ln(\beta/T^{1.8})$ against reciprocal of absolute temperature gives a straight line of which the slope corresponds to $-1.0037\,E/R$. The E can thus be calculated from the slope of the graph.

4. Results and discussion

4.1. Biomass characterization

Table 1 shows the result of the proximate and elemental analyses, and the HHV for the woody and non-woody biomass resources under investigation.

Table 1 shows that SBG has the highest ash content (7.54%) but TI has the least ash content (0.32%) and the highest FCC (17.40%). This is a typical trend with agricultural and forestry samples [2].

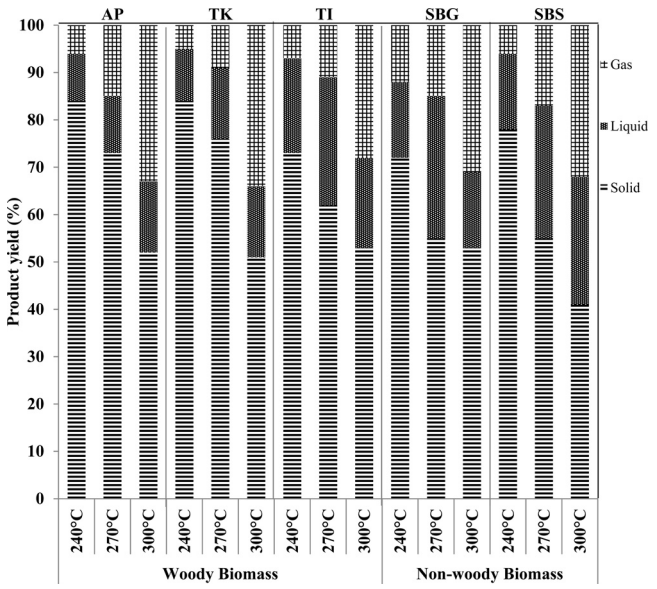

Fig. 2. Torrefaction product yield (%) distribution for various biomass (AP, TK, TI, SBG and SBS) 0.25–0.5 mm particle size and 30 min residence time at 240 °C, 270 °C, and 300 °C.

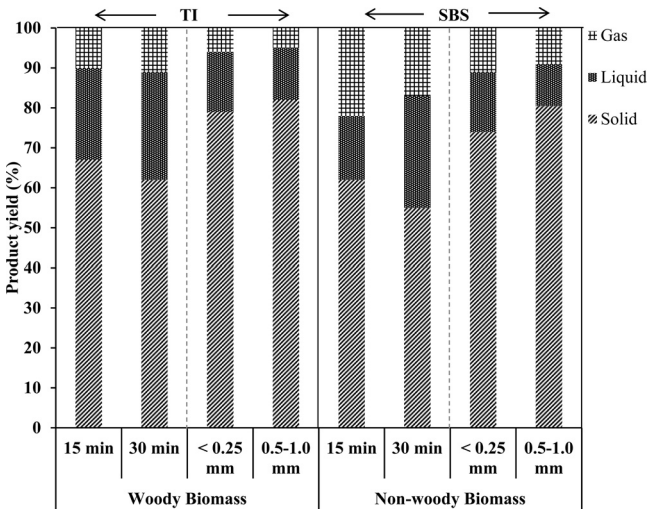

Fig. 3. Torrefaction (270 °C) product yield (%) distribution for TI woody and SBS non-woody biomass at 15 and 30 min residence time and <0.25 and 0.5–1.00 mm particle size.

The VM content for TI (82.3%) and SBG (78.9%) is in consonance with findings in literature wherein Prins et al. [2] reported that VM for beech and switch grass was 82.7% and 79.0% respectively. The data in Table 1 show that the C content for woody biomass was the highest. For instance, AP had 51.65%, while SBG (non-woody) had the least, 42.4%; this is consistent with findings from the literature [30]. The N content for all the samples is ≤1%; this matches results from literature [2,30]. This is a positive sign as there would be a significant reduction in the emission of oxides of N if used for energy generation purposes.

4.2. Torrefaction

Torrefaction is a thermochemical process that allows for the production of high quality char in terms of mass and energy contents. This study examined torrefaction temperatures between 240 and 300 °C.

Fig. 2 presents the product yield (%) distribution during torrefaction experiments at 240, 270, and 300 °C for different biomass samples, while Fig. 3 shows product yield (%) for TI (woody) and SBS (non-woody) biomass samples with respect to varied residence time and particle size. Fig. 2 shows that the highest average solid yield (≈79%) was achieved at 240 °C. A decrease in solid yield was observed resulting in an average of approximately 71% and 58% for woody (AP, TK and TI) and non-woody (SBG and SBS) biomass samples respectively at 270 °C (Fig. 2). It may not be unconnected with the difference in the structural makeup of these classes of biomass as earlier reported by Balogun et al. [31]. Bridgeman et al. [3] made a similar observation of variation in mass yield as a function of biomass type and further alluded to the difference in cell wall composition as a probable explanation. Fig. 3 shows a marginal reduction in solid yield with rise in residence time showing a difference of 4% for woody and 7% for non-woody biomass. Conversely, a minimal increase was seen with higher particle size showing a change of 3% and 6.5% for woody and non-woody biomass respectively. The increase in solid yield with respect to variation in particle size may be due to heat transfer limitation that is usually associated with larger particle size. At relatively smaller particle size, transfer of heat is facilitated as heat is quickly transmitted from the outer to the inner core of the particle leading to a comparatively higher mass diffusion that eventually results in a greater mass loss. The influence of temperature was far more pronounced as the solid yield dropped from 80% at 240 °C to an average of 50% at 300 °C (Fig. 2); this is consistent with the literature [32]. There was a corresponding increase in the volatile yields with increasing temperature. The yield of the volatile product was highest (≈50%) at 300 °C. Prins et al. [2] and Bridgeman et al. [3] reported an increase in volatile yields with temperature and residence time.

4.3. Characterization of torrefied biomass

Once biomass is subjected to a thermochemical process, like torrefaction, it undergoes physical and chemical changes that lead to some transformation in its characteristics.

Fig. 4 shows the change in the VM content between the original biomass and the torrefied samples at 300 °C. There was an average reduction in the VM content of approximately 41% for woody and 53% for non-woody biomass after torrefaction. Bridgeman et al. [3] observed a similar trend in the reduction of VM content between a woody and an agricultural biomass species. A characteristic feature of biomass is its high content of VM. Hence, when subjected to thermochemical conversion technique a substantial part of it is released through devolatilisation [33]; a situation in which volatiles containing varied organic species are liberated either as gaseous or/and liquid components.

Fig. 5 shows the transformation that took place in the FCC after torrefaction between the original and torrefied biomass samples. Fig. 5 reveals an increase in the FCC after torrefaction experiments. A difference of an average of 38% is observed between the FCC for original and torrefied biomass. Ferro et al. [34] reported an increase in the FCC with temperature rise from 230 to 280 °C in torrefaction experiments of agricultural and forestry residues.

Fig. 6 presents a plot of H/C against O/C ratios for original and torrefied biomass samples. The raw biomass samples have high O/C and H/C ratios; greater than 0.6 and 1.3 respectively. The implication is that high volatile and liquid yields can be expected from the thermal treatment of lignocellulosic biomass [35]. Fig. 6 shows that torrefaction leads to a lower O/C ratio (less than an average of 0.3). This trend is consistent with results from literature; Park et al. [14] noted that the O/C ratio for biomass sample dropped from 0.63 to 0.31 after torrefaction. The loss of O in the elemental matrix of biomass is due to the dehydration reaction on the one hand and the formation of CO and CO_2 on the other hand [36]. The

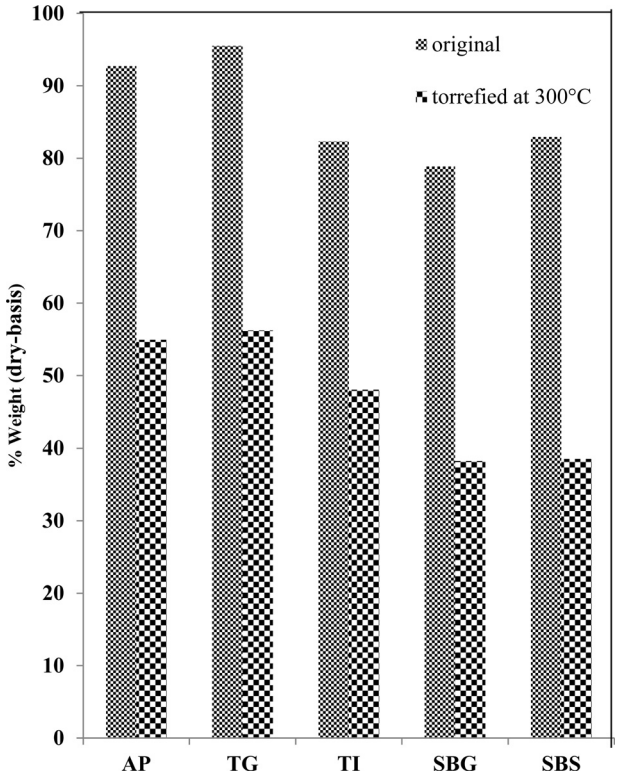

Fig. 4. Volatile matter (VM) content for original and torrefied (at 300 °C) biomass samples.

former is responsible for the formation of water vapour and other organic volatiles, which also results in the reduction of H content. Consequently, there is a significant rise in the C content – a trend attested to by Park et al. [14]. The modification in the elemental configuration brought about by torrefaction makes torrefied biomass acquire thermal and chemical properties that makes it tend toward low rank coal on the van Krevelen diagram [3,37].

Fig. 7 illustrates the variation observed in the HHV for biomass samples after torrefaction experiments. There is a significant change in the energy content of torrefied biomass as a consequence

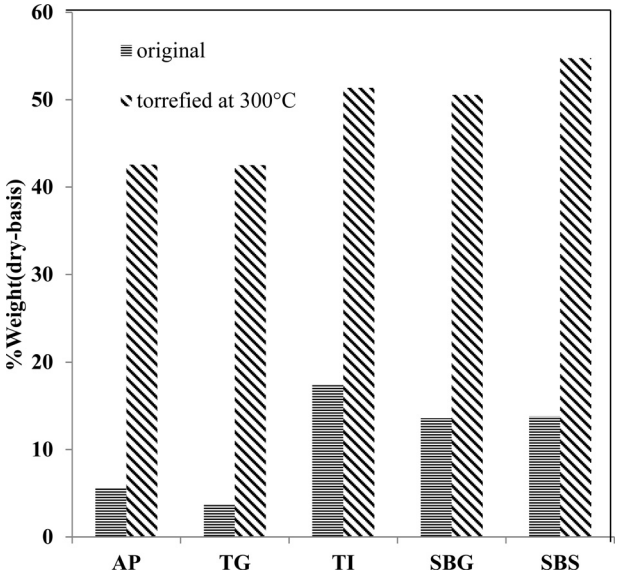

Fig. 5. Fixed carbon content (FCC) for original and torrefied (at 300 °C) biomass samples.

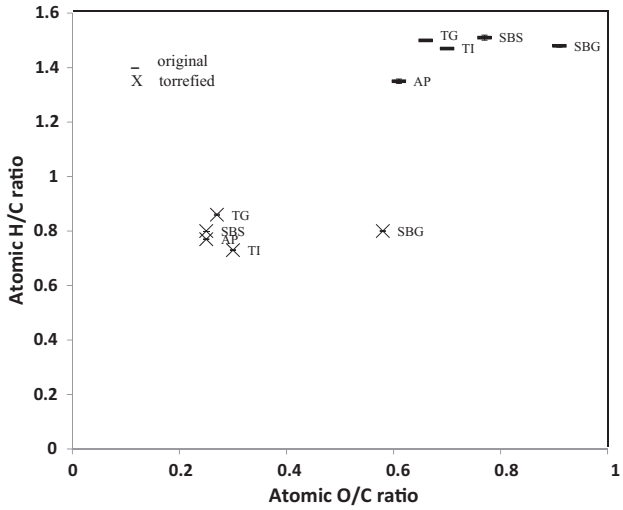

Fig. 6. A plot of H/C against O/C for original and torrefied (at 300 °C) biomass samples.

of the alteration in the elemental configuration earlier discussed (Fig. 6). HHV varied from 19 to 20 MJ kg^{-1} and 16 to 17 MJ kg^{-1} for original woody and non-woody biomass, respectively. Upon torrefaction, the HHV increased from 26 to 27 MJ kg^{-1} and from 24 to 27 MJ kg^{-1} for woody and non-woody biomass, respectively. This trend is similar to observations made in literature [3,12]. Of particular interest, is TI for which a prediction of a probable highest increase in HHV among the woody biomass had been made [31]. Significantly, TI experienced the highest increase in HHV of approximately 38% as compared to AP (32%) and TK (32%). This may be on

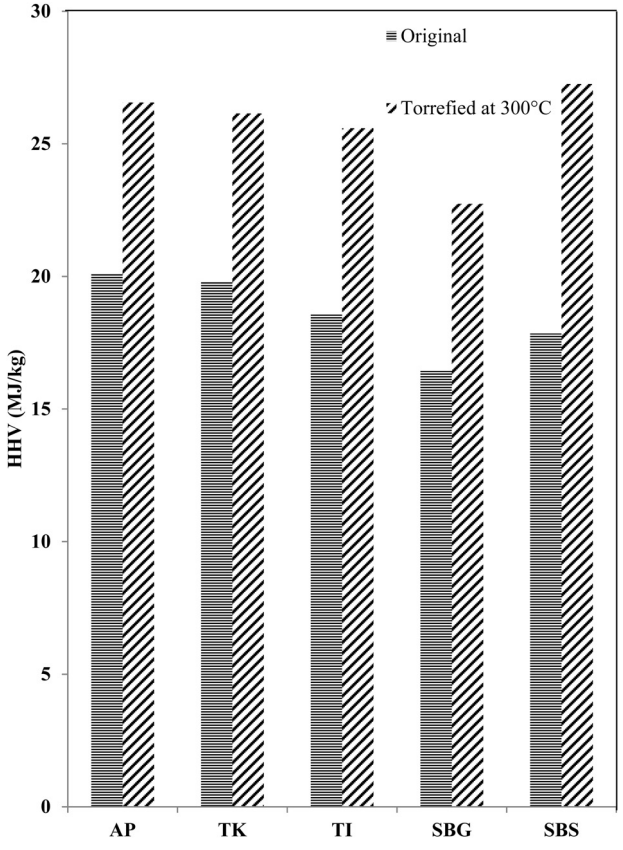

Fig. 7. Variation in HHV between original and torrefied (at 300 °C) biomass samples.

account of the fact that it had the highest lignin content, which is largely unaffected within the temperature range under consideration. More so, it has been established that the influence of lignin on HHV variation is more when compared with extractives in lignocellulosic biomass [38]. Therefore, due to the higher HHV values for TI and torrefied TI [31] it was selected for a thermal degradation kinetic study.

4.4. GC/MS analysis of bio-oil from torrefaction experiments

Torrefaction experiments led to the release of some organic liquid (bio-oil) from the various biomass resources under investigation. The composition of these oils is of immense importance and thus, the bio-oils were analyzed by GC/MS. The results from GC/MS analysis is given in Table 2.

Table 2 presents the GC/MS analysis of the bio-oil released from the torrefaction experiments at 300 °C. A total of 58 compounds were detected in the analysis and more than 50% were identified with the exception of AP, where 38% was identified. The following compounds were detected in all the biomass samples: furfural, guaiacol, 4-methyl guaiacol, 1,4:3,6 dianhydro-glucopyranose, di-anhydro-hexosan, 4-ethylguaiacol, 4-vinyl-guaiacol, syringol, vanillin, trans-isoeugenol, unknown $C_9H_{12}O_3 + C_{10}H_{12}O_2$, 6-hydroxy-hydrocoumarin, guaiacyl acetone, 4-propenyl-syringyl, homo-syringaldehyde, syringyl acetone, hexadecanoic acid and oleic acid.

Woody biomass, TK, has the highest concentration of levoglucosan (7.1%); an intermediate product from the thermal deploymerisation of cellulose [10]. Noticeably, TK has relatively low ash content (Table 1); this may have been responsible for the high yield of levoglucosan. The production of levoglucosan is significantly influenced by the presence of mineral contents in lignocellulosic biomass [10]. It has been established through research that some metals impede the depolymerisation of cellulose and consequently leads to high char and low organic yields, especially levoglucosan in pyrolysis [39,40]. Eom et al. [41] investigated the effect of demineralization on the pyrolytic behavior of biomass. He noted 2–10-fold increase in the concentration of levoglucosan from the demineralized biomass. Another important sugar identified is 1,4:3,6 dianhydro-glucopyranose and it is formed from the dehydration of levoglucosan [10].

The proportion of phenolic organic compounds identified is more than one-third; however, the ones with peak area ≥1.0% and present in all the five samples are guaiacol, 4-ethylguaiacol, syringol, 4-methyl-guaiacol and unknown $C_9H_{12}O_3 + C_{10}H_{12}O_2$. Greenhalf et al. [16] observed that among the group of compounds identified during fast pyrolysis of straw, perennial grasses and hardwoods, phenols constituted about one-third. These are from the deconstruction of lignin fraction and it is consistent with findings from literature [10,17].

4.5. Decomposition kinetics

TI was selected for a thermal degradation kinetic study based on having the highest HHV values after torrefaction, low ash content and high fixed carbon content of the biomass types studied. The results of the TGA measurements were normalized according to the following expression:

$$\alpha = \frac{M_0 - M}{M_0 - M_\infty} \tag{9}$$

where α is conversion ratio, M_0 is initial mass, M_∞ is final residual mass and M is the mass measured by TGA. The thermal decomposition behavior of TI at varied heating rates (5–20 K min^{-1}) is represented by the α and DTG thermograms are shown in Fig. 8. The α curves were obtained by the application

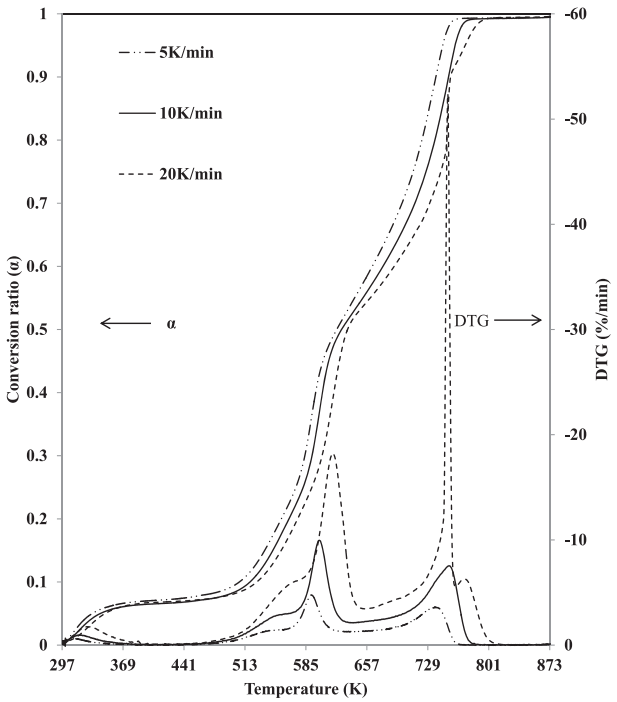

Fig. 8. Conversion ratio (α) and DTG thermograms for TI at heating rates of 5, 10, 20 K min^{-1}.

of Eq. (9). The thermal profiles for biomass decomposition were essentially the same for different heating rates except for successive shifts in the DTG peaks toward higher temperature. For instance, the temperature at maximum DTG peak for 5 K min^{-1}, 10 K min^{-1} and 20 K min^{-1} were 592 K, 600 K and 617 K respectively. This may be due to the fact that rapid heating rate leads to an increase in the temperature gradient between the outer and the inner layer of the test sample. Damartzis et al. [20] and Dash et al. [42] noted that peak temperatures were shifted to higher temperature values with increasing heating rate. Similarly, the α curves moved in the direction of higher temperatures with rising heating rates.

On the DTG thermograms, three stages of decomposition can be distinguished; below 378 K, dehydration reaction and loss of low molar mass organics are observed [43]. Secondly, the main devolatilisation stage (513–657 K) characterized by complex successive and overlapping reactions is seen around the primary peaks; wherein hemicellulose, cellulose and part of lignin are largely degraded. The last stage, seen around the secondary peaks, is suggestive of lignin decomposition since lignin degrades over a broader spectrum of temperature (473–773 K) [44]. It is also noteworthy that a further thermal cracking of some resultant organic compounds, whose formation may have been precipitated in the preceding reactions, could also be responsible. Fisher et al. [45] made reference to the existence of a "secondary thermolysis" at temperature above 673 K. Biagini et al. [46] in offering an explanation for the weight loss events that succeed primary devolatilisation also alluded to the degradation of chemical species that may have been formed during the preceding thermal devolatilisation.

Fig. 9 shows the variation of $E(\alpha)$ as a function of α as determined by FWO and Starink iso-conversional methods; showing data points for α from 0.02 to 0.98 at intervals of 0.02 for TI. An excellent agreement between the two model-free techniques is observed with the difference between them less than 10%. This attests to the validity and reliability of the methods employed for the kinetic parameter determination and this is consistent with results from literature [19,20].

Table 2
GC/MS detectable compounds in bio-oil from torrefaction experiments at 300 °C.

RT (min)	M^+ (m/z)	Compound	AP	TK	TI	SBG	SBS
			Peak area (%)				
4.82	96	Furfural	0.1	1.0	5.1	2.4	0.7
5.27	98	Furfural alcohol	0.1	0.4	–	1.4	1.1
5.64	116	1-Acetyloxy-2-propanone	–	0.7	–	2.3	0.4
6.76	110	1-(2-Furanyl)-ethanone	–	–	0.4	0.3	–
6.84	104	4-Hydroxy-butanoic acid	0.1	–	–	0.9	1.4
7.02	98	1,2-Cyclopentanedione	–	–	–	1.9	0.5
8.12	100	2,3-Pentanedione	–	–	4.5	0.8	–
8.15	110	5-Methyl 2-furaldehyde	–	1.1	–	–	0.9
8.24	110	1-Acetyloxy-2-butanone	–	1.0	–	0.8	0.9
8.68	94	Phenol	–	0.1	0.2	3.2	3.1
9.06	114	2,2-Diethyl-3-methyl-oxazolidine (tentatively)	–	–	–	2.7	0.3
9.24	114	2-Methyl-pentenoic acid	–	–	–	0.4	2.3
9.37	114	2-Methyl-hexen-3-ol	0.6	0.3	0.1	0.6	–
9.93	112	3-Methyl-, -2-cyclopentanedione-	–	1.5	1.2	1.8	2.3
10.29	110	2,3-Dimethyl-2-cyclopenten-1-one	–	0.1	0.1	0.3	0.7
10.76	108 + 126	Methyl phenol + 2-ethyl-2-hydroxy-2-cyclopen-1-one	–	–	0.5	0.5	1.6
11.19	102	Tetrahydro-furfuryl alcohol	–	0.1	–	2.6	2.5
11.32	108	4-Methyl-phenol	–	0.3	–	0.8	1.7
11.74	124	Guaiacol	1.4	2.1	2.8	3.0	3.5
11.86	? + 126	Unknown + 5-methyl-4-hepten-3-one	–	–	–	3.0	2.8
11.99	124	Methoxy-phenol	–	0.7	0.6	–	–
12.36	126	3-Hydroxy-2-methyl-4H-pyran-4-one	0.4	–	–	1.6	0.3
12.56	126	3-Ethyl-2-hydroxy-2-cyclopenten-1-one	–	–	–	0.7	1.5
13.46	134	Eugenol	–	0.1	0.2	0.1	0.7
13.67	128	6-Ethyltetrahydro-2H-pyran-2-one	–	0.7	0.2	0.7	0.2
13.99	122	4-Ethyl-phenol	–	–	0.2	4.4	4.0
14.49	130	Anhydro-pentose	–	2.0	0.7	1.0	0.2
14.67	138	4-Methyl-guaiacol	1.4	4.5	3.2	0.8	1.5
15.17	144	1,4:3,6 Dianhydro-glucopyranose	0.1	0.9	0.6	2.6	1.8
15.46	144	Di-anhydro-hexosan	–	0.4	0.2	1.8	2.7
15.67	144	Di-anhydro-hexosan	0.1	0.7	0.2	0.5	0.6
16.24	132	3-Hydroxy-3-methylpentanoic acid	–	0.4	0.2	3.4	0.3
16.59	140	3-Methoxy-1,2-benzenediol,-	–	0.1	–	0.1	2.1
17.02	152	4-Ethylguaiacol	3.5	3.1	2.0	3.2	3.3
17.98	150	4-Vinyl-guaiacol	2.9	1.3	0.5	2.7	2.5
18.99	154	Syringol	2.4	1.9	7.6	1.4	9.8
19.11	164	Eugenol	2.0	1.5	–	–	–
19.35	164	Cis-isoeugenol	0.6	0.9	1.0	–	–
19.35	166	4-Propyl-guaiacol	–	–	–	0.1	0.4
20.32	152	Vanillin	0.2	0.7	1.0	1.3	0.5
20.42	164	Trans-isoeugenol	0.9	1.0	0.3	0.2	0.5
21.44	168 + 164	$C_9H_{12}O_3$ + $C_{10}H_{12}O_2$ + unknowns	7.1	10.7	5.7	1.0	2.6
21.76	166	Propyl-guaiacol	–	0.5	0.2	–	–
22.33	162	Levoglucosan	–	7.1	2.8	2.2	0.6
23.15	164	6-Hydroxy-hydrocoumarin	0.1	0.4	0.5	3.3	0.1
23.31	182	Ethyl-syringyl	5.2	1.9	1.8	–	1.7
23.46	180	Guaiacyl acetone	0.7	1.4	9.0	0.3	0.8
24.24	180	Vinyl-syringyl	0.4	0.3	–	0.1	0.9
24.66	180	Propioguaiacone	–	0.3	2.0	0.2	0.1
24.80	194	α-Oxy-propioguaiaacone	0.1	–	1.7	0.1	0.1
25.11	194	4-Propenyl-syringyl	1.3	0.8	0.4	1.0	0.4
25.25	196	Homo-syringaldehyde or propylsyringyl	0.8	0.8	0.6	0.3	0.4
28.86	210	Syringyl acetone	1.2	1.6	3.8	0.4	0.8
29.88	210	Propiosyringone	0.2	0.2	1.2	–	0.1
32.45	256	Hexadecanoic acid	0.3	0.1	1.1	0.4	0.4
35.68	284	Oleic acid	0.1	0.1	0.5	0.1	0.3
41.40	272	p-Anisoin	4.6	0.1	–	0.1	–
47.40		Terpene + unknown	0.1	–	–	0.1	–
Total unknown			62.0	47.0	35.8	34.3	31.1

RT, retention time; M^+, molecular ion.

Generally, the complex nature of E dependence on the degree of conversion is demonstrated as $E(\alpha)$ varies continuously with α; rising steadily from around 197 to 363 kJ mol^{-1} at 0.1 and 0.52 respectively (Fig. 9). At this first peak (363 kJ mol^{-1}), the summative input of the three fractions; though in different intensity, is highly suspected. The $E(\alpha)$ subsequently deeps rapidly to 164 kJ mol^{-1} at 0.68 and emerges with a second peak at 0.9 (303 kJ mol^{-1}). This last peak corresponds to the energy barrier that must be overcome in the final degradation stage of the residual lignin [19]. In summary, this illustrates a typical complex decomposition process often characterized by successive, multiple and parallel reaction routes. The respective decomposition stages of biomass fractions have been identified alongside their range of $E(\alpha)$. Subsequent discussion places emphasis on the hemicellulose degradation stage as this is the region associated with torrefaction.

Fig. 9 shows that hemicellulose degradation stage experienced the least range of activation energy (137–197 kJ mol^{-1}). The relatively high reactivity of hemicellulose apparently engenders low activation energy and this is most certainly due to its lack of crystallinity, which is occasioned by its numerous branched polymers

Table 3
Pre-frequency and correlation factors for conversion ratio (α) 0.02–0.98 using FWO method.

α	R^2	$A(\alpha)$ (min^{-1})	α	R^2	$A(\alpha)$ (min^{-1})	α	R^2	$A(\alpha)$ (min^{-1})
0.02	0.995	2.257×10^{15}	0.42	0.980	1.153×10^{16}	0.82	0.992	3.7803×10^{15}
0.04	0.999	4.141×10^{11}	0.44	0.975	3.354×10^{16}	0.84	0.977	2.4668×10^{17}
0.06	0.776	4.886×10^{8}	0.46	0.970	2.151×10^{18}	0.86	0.945	5.6585×10^{18}
0.08	0.810	2.992×10^{4}	0.48	0.973	7.985×10^{21}	0.88	0.896	1.304×10^{20}
0.1	0.975	5.459×10^{12}	0.5	0.992	7.466×10^{25}	0.9	0.857	1.0722×10^{21}
0.12	0.997	3.980×10^{14}	0.52	0.994	7.136×10^{25}	0.92	0.911	4.2448×10^{20}
0.14	0.999	1.271×10^{15}	0.54	0.992	1.489×10^{24}	0.94	0.980	1.0146×10^{18}
0.16	1.000	1.431×10^{15}	0.56	0.999	7.430×10^{18}	0.96	0.997	1.9383×10^{16}
0.18	0.999	4.516×10^{15}	0.58	0.999	1.651×10^{16}	0.98	0.999	3.8018×10^{14}
0.2	0.999	1.396×10^{16}	0.6	1.000	7.905×10^{14}			
0.22	0.999	4.291×10^{16}	0.62	0.999	3.703×10^{13}			
0.24	0.999	1.307×10^{17}	0.64	0.999	1.414×10^{13}			
0.26	0.998	1.432×10^{17}	0.66	0.999	5.261×10^{12}			
0.28	0.996	5.582×10^{16}	0.68	0.998	6.874×10^{11}			
0.3	0.993	2.166×10^{16}	0.7	0.999	2.051×10^{12}			
0.32	0.991	8.283×10^{15}	0.72	0.999	2.138×10^{12}			
0.34	0.988	3.175×10^{15}	0.74	0.999	2.224×10^{12}			
0.36	0.987	3.423×10^{15}	0.76	0.999	2.317×10^{12}			
0.38	0.985	1.281×10^{15}	0.78	0.999	7.008×10^{12}			
0.4	0.981	3.855×10^{15}	0.8	0.999	1.650×10^{14}			

[19]. An increase in $E(\alpha)$ is observed as conversion progresses from 0.1 to 0.24, with a difference of 60 kJ mol^{-1} between the least and the highest value of $E(\alpha)$. Peterson et al. [47] and Valor et al. [48] in offering an explanation for this trend noted that degradation by random scissions of lineal chain which leads to increase in activation energy may have been responsible. The activation energy reaches a peak toward the end of the hemicellulose decomposition and drops gradually into the adjoining stage. This behavior may be as a result of the cross-linking effect associated with hemicellulose and other polymeric constituents yet to be degraded [33]. The value of $E(\alpha)$ obtained for hemicellulose decomposition is similar to findings by Lopez-Velazquez et al. [19] and Wang et al. [49]. The variation in $E(\alpha)$ with conversion reinforces the fact that the decomposition of lignocellulosic biomass follows a complex multiple and competitive reaction paths. Thus, biomass kinetics within the hemicellulose decomposition region can be interpreted as a multi-step mechanism. Prins et al. [7] came to a similar conclusion in which they stated that torrefaction kinetics can best be described by a two-step mechanism.

Table 3 shows the pre-frequency factor (A), the correlation factor R^2 for each slope and conversion ratio. The inconsistency and low correlation seen at α below 0.1 may be due to the fact that the decomposition model adopted for kinetic parameter determination does not accurately capture the physical reaction (dehydration) that is predominant at this stage of decomposition. Chen et al. [50]observed that the early stage of biomass decomposition is a physical reaction; therefore, kinetic models based on chemical reactions are inadequate for kinetic analysis in this stage. The next stage is the hemicellulose degradation region and a high value of R^2 (0.9750–0.9986) between an α of 0.1 and 0.24 was observed. This is an indication that there was a strong correlation for the most part within the decomposition region. This implies that the kinetic data that would be obtained from this data points are reliable. The $A(\alpha)$ varies with conversion having the least value and the highest values as 2.99×10^4 and 7.46×10^{25} min^{-1} at an α of 0.08 and 0.5, respectively.

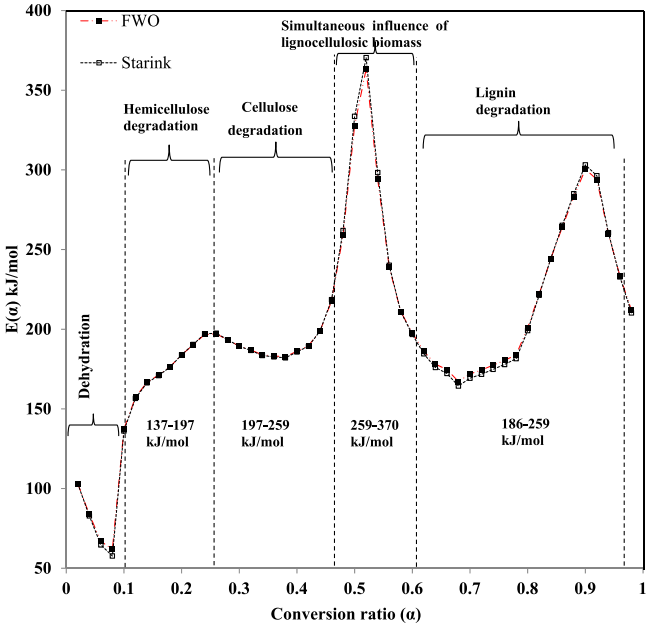

Fig. 9. Activation energy, $E(\alpha)$, as function of the degree of conversion, α, determined from FWO and Starink methods for TI.

5. Conclusion

Biomass type played a significant role in solid yield leading to an average of 71% and 58% yield for woody and non-woody samples respectively at 270 °C. The influence of temperature on solid yield was the most pronounced with a decrease from an average of 80% (at 240 °C) to 50% (at 300 °C) regardless of residence time or particle size. A nominal influence on solid yield with respect to residence time and particle sizes were observed yielding a reduction of about 3.5% and an increase of about 4.6% respectively.

A decline of about 41% and 53% in the content of volatile matter for woody and non-woody biomass respectively was seen after torrefaction. There was also a phenomenal rise in the fixed carbon contents (an average of 38% difference) for torrefied biomass. The change in the elemental matrix of torrefied biomass was evident with O/C ratio dropping from 0.6 to 0.3. Thus, torrefied biomass acquired thermal and chemical properties that made it tend more toward low rank coal on the van Krevelen diagram. Conclusively, TI, among the woody biomass experienced the highest increase in HHV of approximately 38% as compared with AP (32%) and TK (32%).

Levoglucosan, a product of cellulose depolymerization, had the highest concentration (7.1%) in woody biomass, while phenolic compounds made up more than one-third of the group of compounds identified.

The decomposition parameters showed a shift toward higher values as heating rate increases. The dependence of activation energy on degree of conversion was also demonstrated as $E(\alpha)$ varies continuously with α for TI which is the biomass of choice for kinetic study. The activation energy for the hemicellulose degradation stage for TI ranged between 137 and 197 kJ mol^{-1} for conversion between 0.1 and 0.24. By implication biomass kinetics within the hemicellulose decomposition region can thus be said to be a multi-step reaction.

Acknowledgement

We acknowledge the financial support from the Lower Niger River Basin Development Authority sponsorship program.

References

[1] M.J.C. van der Stelt, H. Gerhauser, J.H.A. Kiel, K.J. Ptasinski, Biomass upgrading by torrefaction for the production of biofuels: a review, Biomass Bioenergy 35 (9) (2011) 3748–3762.
[2] M.J. Prins, K.J. Ptasinski, F.J.J.G. Janssen, Torrefaction of wood: Part 2: analysis of products, J. Anal. Appl. Pyrolysis 77 (2006) 35–40.
[3] T.G. Bridgeman, J.M. Jones, I. Shield, P.T. Williams, Torrefaction of reed canary grass, wheat straw and willow to enhance solid fuel qualities and combustion properties, Fuel 87 (2008) 844–856.
[4] J.P. Bourgeois, J. Doat, Torrefied wood from temperate and tropical species: advantages and prospects. Proceedings of an International Conference on Bioenergy in Göteborg, Bioenergy 84 (3) (1985) 153–159.
[5] M. Pach, R. Zanzi, E. Björnbom, Torrefied biomass as substitute for wood and charcoal, in: Proceedings of the Sixth Asia-Pacific International Symposium on Combustion and Energy Utilization, Kuala Lumpur, Malaysia, May 20–22, 2002.
[6] P. Girard, N. Shah, Developments on torrefied wood: an alternative to charcoal, REUR Tech. Ser. Charcoal Prod. Pyrol. Technol. 20 (1991) 101–114.
[7] M.J. Prins, K.J. Ptasinski, F.J.J.G. Janssen, Torrefaction of wood: Part 1: weight loss kinetics, J. Anal. Appl. Pyrolysis 77 (1) (2006) 28–34.
[8] E. Diaz, T. Smith-Sivertsen, R.T. Lie, D. Pope, N. Bruce, A. Diaz, J. McCracken, B. Arana, K.R. Smith, Eye discomfort, headache and back pain among Mayan Guatemalan women taking part in a randomized stove intervention trial, J. Epidemiol. Commun. Health 61 (1) (2007) 74–79, http://dx.doi.org/10.1136/jech.2006.043133.
[9] M. Guggisberg, P.A. Hassel, D. Michaelchuk, J. Ahmad, Respiratory symptoms and exposure to wood smoke in an isolated Northern Community, Can. J. Public Health 94 (5) (2003) 372–376.
[10] A.M. Azeez, D. Meier, J. Odermatt, T. Willner, Fast pyrolysis of African and European lignocellulosic biomasses using Py-GC/MS and fluidized bed reactor, Energy Fuels 24 (2010) 2078–2085.
[11] Y.S. Mohammed, M.W. Mustafa, N. Bashir, A.S. Mokhtar, Renewable energy resources for distributed power generation in Nigeria: a review of the potential, Renew. Sustain. Energy Rev. 22 (2013) 257–268.
[12] B. Arias, C. Pevida, J. Fermoso, M.G. Plaza, F. Rubiera, J.J. Pis, Influence of torrefaction on grindability and reactivity of woody biomass, Fuel Process. Technol. 89 (2008) 169–175.
[13] J.S. Tumuluru, S. Sokhansanj, C.T. Wright, R.D. Boardman, Biomass Torrefaction Process Review and Moving Bed Torrefaction System Model Development, U.S. Department of Energy National Laboratory, 2010.
[14] J. Park, J. Meng, K.H. Lim, O.J. Rojas, S. Park, Transformation of lignocellulosic biomass during torrefaction, J. Anal. Appl. Pyrolysis 100 (2013) 199–206.
[15] M. Crocker, R. Andrews, The rationale for biofuels, in: P. Lawrence (Ed.), Thermochemical Conversion of Biomass to Liquid Fuels and Chemicals, RSC Publishing, Cambridge, 2010.
[16] C.E. Greenhalf, D.J. Nowakowski, A.B. Harms, J.O. Titiloye, A.V. Bridgwater, A comparative study of straw, perennial grasses and hardwoods in terms of fast pyrolysis products, Fuel 108 (2013) 216–230.
[17] N. Gao, A. Li, C. Quan, L. Du, Y. Duan, TG-FTIR and Py-GC/MS analysis on pyrolysis and combustion of pine sawdust, J. Anal. Appl. Pyrolysis 100 (2013) 26–32.
[18] A. Charles, A. Mullen, A. Boateng, Chemical composition of bio-oils produced by fast pyrolysis of two energy crops, Energy Fuels 22 (2008) 2104–2109.
[19] M.A. Lopez-Velazquez, V. Santesa, J. Balmased, E. Torres-Garciac, Pyrolysis of orange waste: a thermo-kinetic study, J. Anal. Appl. Pyrolysis 99 (2013) 170–177.
[20] T.H. Damartzis, D. Vamvuka, S. Sfakiotakis, A. Zabaniotou, Thermal degradation studies and kinetic modeling of cardoon (*Cynara cardunculus*) pyrolysis using thermogravimetric analysis (TGA), Bioresour. Technol. 102 (2011) 6230–6238.
[21] C. Gai, Y. Dong, T. Zhang, The kinetic analysis of the pyrolysis of agricultural residue under non-isothermal conditions, Bioresour. Technol. 127 (2013) 298–305.
[22] British Standards Institution. BS EN 15148:2009, Solid Biofuels: Determination of the Content of Volatile Matter, BSI, London, 2009.
[23] American Standard of Testing and Materials. ASTM D1102-84, Standard Test Method for Ash in Wood, ASTM International, 1984, West Conshohocken, PA, 2007.
[24] American Standard of Testing and Materials. ASTM D5865-04, Standard Test Method for Gross Calorific Value of Coal and Coke, ASTM International, West Conshohocken, PA, 2004.
[25] K.V. Pillai, A.G. McDonald, F.G. Wagner, Developing a model system in vitro to understand tracheary element development in Douglas-fir (*Pseudotuga mensziesii*), Maderas Cienc. Tecnol. 13 (1) (2011) 3–18.
[26] A.J. Soria, A.G. McDonald, S.J. Shook, Wood solubilization and depolymerization using supercritical methanol. Part 1: process optimization and analysis of methanol insoluble components (bio-char), Holzforschung 62 (2008) 402–408.
[27] C.D. Doyle, Series approximations to the equations of thermogravimetric data, Nature 207 (1965) 290–291.
[28] J.H. Flynn, The iso-conversional method for determination of energy of activation at constant heating rates, J. Therm. Anal. 27 (1983) 95–102.
[29] M.J. Starink, A new method for the derivation of activation energies from experiments performed at constant heating rate, Thermochim. Acta 288 (1996) 97–104.
[30] S. Naik, V.V. Goud, P.K. Rout, K. Jacobson, A.K. Dalai, Characterisation of Canadian biomass for alternative renewable biofuel, Renew. Energy 35 (2010) 1624–1631.
[31] A.O. Balogun, O.A. Lasode, A.G. McDonald, Thermo-analytical and physico-chemical characterization of woody and non-woody biomass from an agro-ecological zone in Nigeria, Bio Resources 9 (3) (2014) 5099–5113.
[32] Y. Uemura, W. Omat, N.A. Othman, S. Yusup, Tsutsui, Torrefaction of oil palm EFB in the presence of oxygen, Fuel 103 (2013) 156–160.
[33] S. Gaur, T.B. Reed, Thermal Data for Natural Synthetic Fuels, Marcel Dekker, New York, 1998.
[34] D. Ferro, V. Vigouroux, A. Grimm, Torrefaction of agricultural and forest residues, in: Cubasolar 2004, April 12–16, Guantánamo, Cuba, 2004.
[35] P. Basu, Biomass Gasification and Pyrolysis: Practical Design and Theory, Academic Press, California, 2010.
[36] M.J. Prins, K.J. Ptasinski, F.J.J.G. Janssen, More efficient biomass gasification via torrefaction, Energy 31 (2006) 3458–3470.
[37] P. Rousset, C. Aguiar, N. Labbe, J.M. Commandre, Enhancing the combustible properties of bamboo by torrefaction, Bioresour. Technol. 102 (2011) 8225–8231.
[38] C. Telmo, J. Lousada, The explained variation by lignin and extractive contents on higher heating value of wood, Biomass Bioenergy 35 (2011) 1663–1667.
[39] G. Dobele, G. Rossinskaja, T. Diazbite, G. Telyshrva, D. Meier, O. Faix, Application of catalysts for obtaining 1,6-anhydrosaccharides from cellulose and wood by fast pyrolysis, J. Anal. Appl. Pyrolysis 74 (2005) 401–405.
[40] G.N. Richards, G.C. Zheng, Influence of metal-ions and of salts on products from pyrolysis of wood: applications to thermochemical processing of newsprint and biomass, J. Anal. Appl. Pyrolysis 21 (1991) 133–146.
[41] I. Eom, K. Kim, J. Kim, S. Lee, H. Yeo, I. Choi, J. Choi, Characterization of primary thermal degradation features of lignocellulosic biomass after removal of inorganic metals by diverse solvents, Bioresour. Technol. 102 (3) (2011) 3437–3444.
[42] M. Dash, V.V. Dasu, K. Mohanty, Non-isothermal kinetic study of three lignocellulosic biomass using model-free methods, J. Renew. Sustain. Energy (2013), http://dx.doi.org/10.1063/1.48302685063101.
[43] V. Tihay, P. Gillard, Pyrolysis gases released during the thermal decomposition of three Mediterranean species, J. Anal. Appl. Pyrolysis 88 (2) (2010) 168–174.
[44] T. Wongsiriamnuay, N. Tippayawong, Non-isothermal pyrolysis characteristics of giant sensitive plants using thermogravimetric analysis, Bioresour. Technol. 101 (2010) 5638–5644.
[45] T. Fisher, M. Hajaligol, B. Waymack, D. Kellogg, Pyrolysis behaviour and kinetics of biomass derived materials, J. Anal. Appl. Pyrolysis 62 (2) (2002) 331–349.
[46] E. Biagini, A. Fantei, L. Tognotti, Effect of the heating rate on the devolatilization of biomass residues, Thermochim. Acta 472 (2008) 55–63.
[47] J.D. Peterson, S. Vyazovkin, C.A. Wight, Kinetics, of the thermal and thermo-oxidative degradation of polystyrene, polyethylene and poly(propylene), Macromol. Chem. Phys. 202 (2001) 775–784.
[48] A. Valor, S. Kycia, E. Torres-Garcia, E. Reguera, C. Vazquez-Ramos, F. Sanchez-Sinencio, Structural and thermal study of calcium undecanoate, J. Solid State Chem. 172 (2003) 471–479.
[49] G. Wang, W. Li, B. Li, H. Chen, TG study on pyrolysis of biomass and its three components under syngas, Fuel 87 (2008) 552–558.
[50] D. Chen, Y. Zheng, X. Zhu, In-depth investigation on the pyrolysis kinetics of raw biomass. Part I: kinetic analysis for the drying and devolatilization stages, Bioresour. Technol. 131 (2013) 40–46.